

Electron nuclear double resonance with donor-bound excitons in silicon

David P. Franke,^{1,*} Michael Szech,¹ Helge Riemann,² Nikolai V. Abrosimov,² Peter Becker,³ Hans-Joachim Pohl,⁴ Kohei M. Itoh,⁵ Michael L. W. Thewalt,⁶ and Martin S. Brandt¹

¹Walter Schottky Institut and Physik-Department,

Technische Universität München, 85748 Garching, Germany

²Leibniz-Institut für Kristallzüchtung, 12489 Berlin, Germany

³PTB Braunschweig, 38116 Braunschweig, Germany

⁴VITCON Projectconsult GmbH, 07743 Jena, Germany

⁵School of Fundamental Science and Technology, Keio University, Yokohama 223-8522, Japan

⁶Simon Fraser University, Burnaby, British Columbia V5A 1S6, Canada

We measure electron nuclear double resonance (ENDOR) of phosphorus in isotopically purified ^{28}Si by optical-electrical hybrid detection via the donor-bound exciton transitions. This allows for the control of both nuclear and electron spin of donors in samples, where the hyperfine splitting is not resolved in the optical spectrum and hence significantly relaxes the requirements on the experimental setup.

Spin-to-charge conversion in electrically detected magnetic resonance provides a very sensitive way of measuring the spins of donors in silicon [1–4], enabling the detection of single spins [5, 6], as well as spin resonance experiments at low or zero external magnetic field [7–9]. In the context of quantum computation, where the electron and nuclear spins of donors in silicon are interesting because of their extremely long coherence times [4, 10–13], electrical detection, as well as electrical control [14–17], could facilitate an integration of quantum bits with current semiconductor technology. In the case of electrical detection based on spin-dependent recombination, the time scales which can be addressed can be limited by the spin lifetime of the particular readout partner [8, 18] which in turn also limits the nuclear spin coherence time of neutral donors [19, 20]. The spin-to-charge conversion based on the creation of donor-bound excitons (DBE), on the other hand, does not have this effect [4]. DBE complexes can be formed by resonant infrared laser excitation and almost immediately decay in an Auger process generating nonequilibrium charge carriers in the conduction band, allowing the detection of the optical transition as a photocurrent. In particular in isotopically purified ^{28}Si , these infrared transitions can be remarkably sharp and the Zeeman interaction of the donor and the DBE complex with magnetic fields can be resolved in the optical spectra [21, 22]. This spin-selective excitation can be used as an electrical detection mechanism for the electron spin of the donor [22], called Auger-electron-detected magnetic resonance (AEDMR) [4]. In samples with high purity and at low temperatures (typically $T < 5$ K), it is even possible to optically resolve the hyperfine splitting [22, 23] enabling the optical [24, 25] and electrical [4] detection of the nuclear spin state.

To avoid straining the sample, in these experiments the photoconductivity is usually monitored in a contactless capacitive fashion by placing it between two metal plates and measuring their impedance. Recently, the

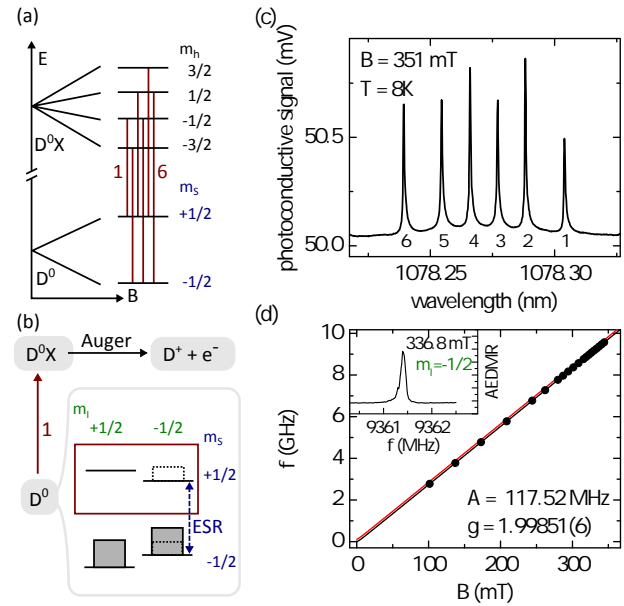


FIG. 1. (a) Level scheme showing the donor-bound exciton transitions. (b) Level population scheme demonstrating the principle of the AEDMR detection. For details see text. (c) Photoconductive spectrum at $B = 351$ mT showing the six electron-spin-selective transitions. (d) Frequency of the $m_I = -1/2$ resonance as a function of the magnetic field B . Solid black and red lines represent calculated $m_I = -1/2$ and $m_I = +1/2$ peak positions, respectively, for $g = 1.99851$ and $A = 117.52$ MHz.

AEDMR detection of the electron spin of ^{31}P donors was realized in samples equipped with evaporated Al contacts [26]. While this experimental realization allows for a higher sensitivity compared to a capacitive detection of the sample's conductivity, the strain induced by the contact structure appears to significantly shift and broaden the DBE transitions, inhibiting the separation of the nuclear spin states in that study. We address this

issue by implementing Auger-electron-detected electron nuclear double resonance (ENDOR), enabling us to detect the nuclear spin state of ^{31}P donors in experimental conditions such as higher temperatures or the presence of strain, where the hyperfine interaction is not optically resolved.

A schematic representation of the DBE transitions (not considering the hyperfine interaction) is shown in Fig. 1 (a). The neutral donor states are labeled D^0 and split up in two levels with electron spin projections $m_S = \pm 1/2$ due to the Zeeman interaction with an external magnetic field B . The donor-bound exciton states, labeled D^0X , split according to the Zeeman interaction of the hole with spin $3/2$ and spin projections $m_h = -3/2 \dots 3/2$, since the two electrons in the three-particle DBE complex form a spin singlet. This leads to a total of six dipole-allowed optical transitions indicated by the red lines labeled 1 through 6 [22].

The selective excitation of one of these lines allows us to perform electrically detected ESR experiments, as schematically shown in Fig. 1 (b), where the laser is assumed to excite DBE line 1. The ionization of donors in the $m_S = +1/2$ state and the subsequent capture of an electron with random spin state lead to an accumulation of donors with $m_S = -1/2$ and hence a large steady-state polarization. The level populations of the neutral donors D^0 with electron and nuclear spin projections m_S and m_I , resp., are shown by the gray boxes in Fig. 1 (b). Since the ESR transitions, in contrast to the DBE transitions in our experiments, are nuclear-spin-selective, all four donor levels have to be considered when discussing the principle of the AEDMR experiments. If one of the two ESR transitions ($\Delta m_S = \pm 1$, $\Delta m_I = 0$) is saturated by microwave (mw) irradiation (dashed blue arrow), one of the $m_S = +1/2$ states gets repopulated (dashed boxes). Under continuous excitation of one of the DBE lines (here: DBE line 1), the ESR saturation enhances the formation of DBEs and, subsequently, the ejection of charge carriers into the conduction band. It is easily seen that, while shown for DBE line 1 and $m_I = -1/2$ here, this process can realize an electrical detection of ESR for all six DBE lines and both ESR transitions.

The experiments are performed on an isotopically purified ^{28}Si sample ($[^{28}\text{Si}] = 99.995\%$) with a dopant concentration $[\text{P}] = 8 \times 10^{14} \text{ cm}^{-3}$ in a Bruker flexline X-band resonator for pulsed ENDOR in a He-flow cryostat at a typical temperature $T = 6 \text{ K}$. To avoid mechanical stress, the sample is mounted loosely between two gold-covered plates, the impedance of which is monitored at 476 kHz with a lock-in amplifier. The phase of the detection is chosen such that the signal-to-noise ratio of the photoconductivity measurement is optimal. The magnetic field was calibrated with an NMR Gaussmeter placed at the sample position, giving an estimated uncertainty of $\pm 0.01 \text{ mT}$. A NKT Photonics fiber laser with power $P = 15 \text{ mW}$ is focused on the sample's edge. For continuous

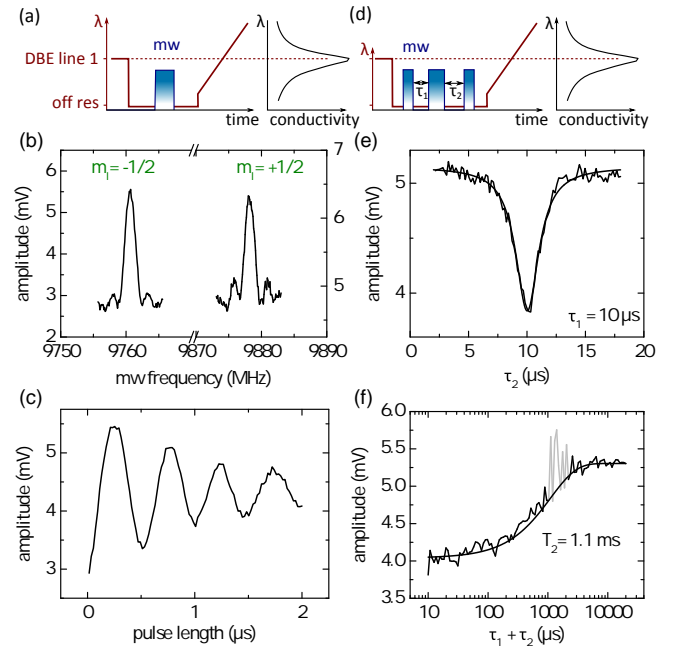


FIG. 2. Auger-detected electron spin resonance experiments. (a) Pulse sequence showing the laser tuning (red line) and an mw pulse (blue), as well a typical conductivity trace. (b) Resonance spectra and (c) Rabi oscillations of the ^{31}P electron spin. (d) Pulse sequence used for electron spin echo experiments. (e) Echo for $\tau_1 = 10 \mu\text{s}$, (f) echo decay, revealing a coherence time $T_2 = 1.1 \text{ ms}$. The data points shown in gray have been excluded from the exponential fit.

wave (cw) ESR measurements, the laser wavelength is tuned to one of the DBE lines and stabilized by a PI controller using the observed photoconductivity as feedback.

Figure 1 (c) exemplarily shows the measured photoconductive signal as a function of the laser wavelength and clearly shows the six DBE lines which are split by an external magnetic field $B = 351 \text{ mT}$. Tuning the laser to DBE line 1 and sweeping the mw frequency f at a fixed external magnetic field, we record AEDMR spectra. A typical AEDMR spectrum is shown in the inset of Fig. 1 (d), where the photoconductive signal is shown as a function of the mw frequency for $B = 336.8 \text{ mT}$. Due to the long coherence times of the electron spin, only weak microwave powers are needed to saturate the ESR transition. Therefore, in cw experiments, we are able to use the microwave antenna of the X-band resonator as a broadband mw delivery system, allowing us to perform measurements over a large frequency and magnetic field range. The observed resonance positions are shown as circles in Fig. 1 (d) and the theoretically expected positions for the low frequency ($m_I = -1/2$) peak are fit to the data (black line). With the hyperfine interaction constant $A = 117.52 \text{ MHz}$ as determined by the EN-

ENDOR experiments below, the fit results in an electronic g-factor $g = 1.99851(6)$, which is in very good agreement with previous measurements [27].

To perform pulsed ESR measurements, we use the piezotuning of the laser to switch between on-resonance and off-resonance illumination. A typical pulse sequence is shown in Fig. 2(a), where the laser tuning during the sequence is indicated by the red line, schematically showing the laser wavelength λ on the vertical axis. After a long (typically 1s) polarization period (here DBE line 1), the laser is tuned off-resonance to avoid spurious ionization during the manipulation of the spin system via magnetic resonance. Then, one or more microwave pulses are applied. At the end of each sequence, the laser wavelength is swept over the DBE resonance line. A typical photoconductive trace as measured after the application of a resonant mw pulse is shown as a function of λ at the right of the sequence. The amplitude of the observed line is determined by fitting the trace with a Lorentzian and is a measure for the population of the probed donor state (here $m_S = +1/2$). Note that the strong DBE signal allows us to perform all experiments single-shot, without additional averaging. Furthermore, this approach provides an easy and frequent calibration of the position of the DBE line to compensate for slow drifts in the laser wavelength or changes in the magnetic field.

We now use the mw resonator close to its resonance frequency, which at the applied mw power leads to a π pulse length of ~ 250 ns, and again set the magnetic field to $B = 351$ mT. Sweeping the frequency of the mw pulse within the flat region of the detuned resonator, ESR spectra are recorded, which show the two hyperfine-split resonance peaks [Fig. 2(b)]. As expected and analogous to the cw measurements, the photoconductivity is enhanced on resonance, where a repopulation of the $m_S = +1/2$ level is achieved (cf. Fig. 1 (b)). The lineshape is limited by the excitation bandwidth of the mw pulse. By changing the length of the mw pulse, Rabi oscillations are recorded as shown in Fig. 2 (c), demonstrating that the coherent control of the electron spin can be detected. For the detection of an electron spin echo, the single pulse is replaced by an echo sequence $\pi/2 - \tau_1 - \pi - \tau_2 - \pi/2$ which includes a final $\pi/2$ pulse [28, 29] to project the magnetization onto the z -axis where it can be detected by the AEDMR readout [Fig. 2(d)]. The resulting spin echo is shown in Fig. 2(e) for $\tau_1 = 10 \mu\text{s}$. We can measure the electron spin coherence time T_2 by recording the echo amplitude as a function of $\tau_1 + \tau_2$ for $\tau_1 = \tau_2$, which is shown in Fig. 2(f), and find a $T_2 = 1.1 \text{ ms}$, comparable to similar measurements on isotopically purified ^{28}Si [11, 26].

For the detection and coherent manipulation of the nuclear spin, we combine mw and radio frequency (rf) pulses to implement Auger-detected ENDOR. We discuss our experimental approach with the help of Fig. 3, where the applied pulse sequence is shown in (a) together with

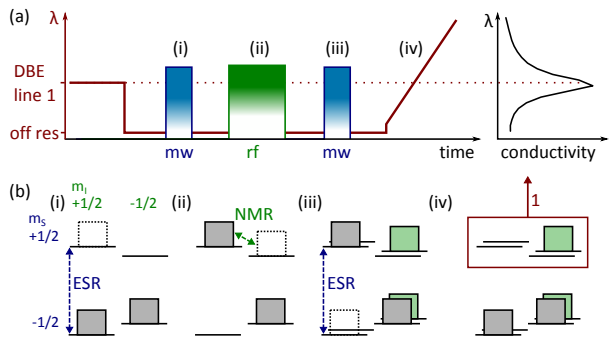


FIG. 3. Schematic representation of the Auger-electron-detected ENDOR experiments. (a) Pulse sequence showing the laser tuning (red line), the mw (blue) and rf (green) pulses, as well as a typical conductivity trace. (b) Level population diagram at points (i)-(iv) indicated in (a). Boxes represent the level populations before (solid boxes) and after (dashed boxes) the mw and rf transitions indicated by blue and green dashed arrows, respectively.

level schemes illustrating the population of the donor spin states during the experiment in (b). At the beginning, the resonant laser excitation (DBE line 1) once more polarizes the system by ionization of the donors with $m_S = +1/2$. As a result, only the $m_S = -1/2$ states are occupied as depicted by the gray boxes in Fig. 3 (b)(i). After the laser is tuned off-resonance, a selective mw π pulse swaps the populations of the two $m_I = +1/2$ states (dashed blue arrow). If a resonant rf pulse is applied (dashed green arrow in (ii)), a transition within the $m_S = +1/2$ subensemble is induced. Panel (iii) shows the level populations after such an NMR pulse by the green boxes; if the rf pulse is off-resonance, the populations remain unchanged (gray boxes). Then, a second mw π pulse is applied (dashed blue arrow in (iii)), which again swaps the populations of the two $m_I = +1/2$ states. The resulting configuration is different, depending on whether a resonant rf pulse has been applied in (ii). In the case of no resonant rf pulse (gray boxes), the mw pulse swaps the populations back to their initial state. Starting from a configuration after a resonant rf pulse (green boxes), however, the second mw pulse has no effect on the populations, since it is between two empty levels. Therefore, in the case of a resonant rf pulse, one of the $m_S = +1/2$ levels remains occupied after the second mw pulse, while otherwise their population is small (cf. (iv)). At the end of the sequence, the laser wavelength is again swept and reveals the signal for DBE line 1, measuring the population of the $m_S = +1/2$ states (red frame in (b)(iv)). Its magnitude is therefore enhanced in the case of a resonant rf pulse (green boxes). In principle, both NMR transitions can be measured using the same DBE line for polarization and detection of the spin ensemble. This

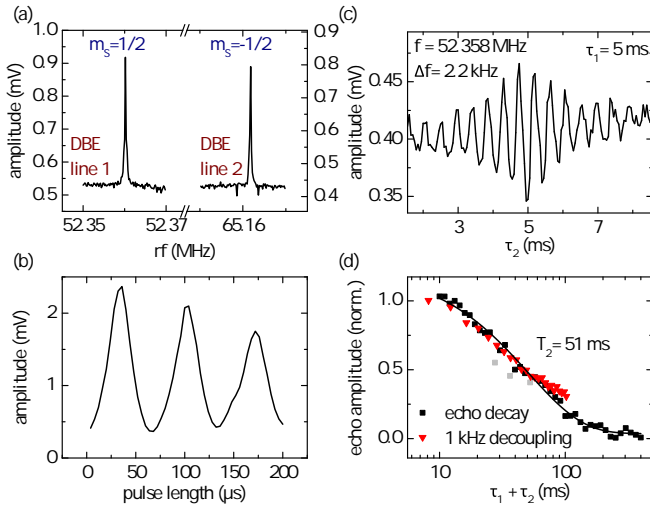


FIG. 4. (a) Auger-electron-detected ENDOR spectrum showing the two ^{31}P nuclear spin resonances. (b) Rabi oscillations of the nuclear spin. (c) Nuclear spin echo. The rf pulses are slightly off resonance ($\Delta f \approx 2.2$ kHz). (d) Nuclear spin echo decay, which is well described by an exponential decay (black line), revealing a coherence time $T_2 = 51$ ms, which is not significantly changed by the application of dynamical decoupling pulses (red triangles).

becomes clear from Fig. 3 (b). The application of an rf pulse resonant with the $m_S = -1/2$ subensemble populates the $m_S = -1/2$, $m_S = +1/2$ level, meaning that the final mw π pulse is between two equally occupied levels. Similar to the case discussed above, this leads to a remaining occupation of one of the $m_S = +1/2$ levels and hence to a photoconductive signal.

For the experimental realization of the measuring scheme, we use the $m_I = +1/2$ ESR transition at 9760 MHz and $B = 351$ mT. In Fig. 4 (a), the resulting ENDOR signal is shown as a function of the frequency of the applied rf pulse. Two peaks are observed, corresponding to the resonances of the $m_S = +1/2$ and $-1/2$ subensembles. The line positions correspond to a hyperfine interaction of $A = 117.52(2)$ MHz and a nuclear g -factor $g_n = 2.259(2)$, in very good agreement with previous measurements [24, 27]. As mentioned, both nuclear spin resonances can be detected with the excitation of the same DBE line. However, we have found that driving the NMR transition between the two levels that are not ionized by the laser leads to very long polarization lifetimes (> 1 min) and significant broadening of the spectrum even when a $\pi/2$ reset pulse is added to the sequence. Therefore, we have used DBE line 2 which ionizes the $m_S = -1/2$ states for the detection of the resonance at 65.162 MHz.

By changing the length of the applied rf pulse, we are able to record Rabi oscillations of the nuclear spin which are shown in Fig. 4(b). Replacing the single rf pulse by a

three-pulse echo sequence equivalent to the electron spin echo sequence shown in Fig. 2 (c), a nuclear spin echo is recorded for $\tau_1 = 5$ ms [Fig. 4(c)]. The echo displays an oscillation with $\Delta f \approx 2.2$ kHz, revealing a slight offset of the applied rf pulses from the NMR transition. The width of the observed echo (~ 4 ms) corresponds to a linewidth of about 250 Hz, suggesting that the spectra in Fig. 4 (a) are also limited by the excitation bandwidth of the applied pulses (pulse length 3.5 ms)

To determine the nuclear spin coherence time, we measure the echo amplitude as a function of $\tau_1 + \tau_2$. The observed decay is well described by an exponential decay with a time constant $T_2 = 51$ ms. It is not significantly enhanced by the application of dynamical decoupling pulses, as shown by the red triangles in Fig. 4 (d), where refocusing pulses are applied at a frequency $f_\pi = 1.01$ kHz in a Carr-Purcell sequence [30]. This suggests that the coherence time is limited by a process that is either frequency independent or cannot be refocused and is in agreement with the observation of an exponential decay in Fig. 4 (d) [31]. We therefore suspect that electron spin flip-flop processes limit the nuclear spin coherence time in this sample because of the rather large phosphorus concentration.

In summary, we have demonstrated Auger-electron-detected ENDOR measurement allowing for the detection and manipulation of the nuclear spin state of phosphorus donors in samples and experimental settings, where the optical selectivity on m_I is not provided. This approach significantly lowers the requirements on the linewidth of the laser used for excitation, on strain and isotopic purity of the sample, and on the experimental temperature compared to Auger-electron-detected NMR experiments. In addition, we have exploited the long electron spin coherence time to realize AEDMR experiments even with very weak mw power which is provided by the antenna of a dielectric resonator used at frequencies far from its resonance. Since the DBE transitions also split in silicon with natural isotope composition [32], the discussed ENDOR technique can enable the control of the ^{31}P nuclear spin in such samples as well. The resulting very large polarization can also be transferred to ^{29}Si nuclear spins to enhance the NMR signal in Si nanoparticle MRI agents [33].

This work was financially supported by DFG through SPP 1601 (Grant Br 1858/8-2) and the JST-DFG Strategic Cooperative Program on Nanoelectronics, the work at Keio was supported by KAKENHI (S) No. 26220602, JSPS Core-to-Core Program, and the Spintronics Research Network in Japan.

* david.franke@wsi.tum.de

[1] A. R. Stegner, C. Boehme, H. Huebl, M. Stutzmann,

K. Lips, and M. S. Brandt, *Nature Phys.* **2**, 835 (2006).

[2] D. R. McCamey, H. Huebl, M. S. Brandt, W. D. Hutchinson, J. C. McCallum, R. G. Clark, and A. R. Hamilton, *J. Appl. Phys.* **89**, 182115 (2006).

[3] D. R. McCamey, J. V. Tol, G. W. Morley, and C. Boehme, *Science* **330**, 1652 (2010).

[4] M. Steger, K. Saeedi, M. L. W. Thewalt, J. J. L. Morton, H. Riemann, N. V. Abrosimov, P. Becker, and H.-J. Pohl, *Science* **336**, 1280 (2012).

[5] A. Morello, J. J. Pla, F. A. Zwanenburg, K. W. Chan, K. Y. Tan, H. Huebl, M. Möttönen, C. D. Nugroho, C. Yang, J. A. v. Donkelaar, A. D. C. Alves, D. N. Jamieson, C. C. Escott, L. C. L. Hollenberg, R. G. Clark, and A. S. Dzurak, *Nature* **467**, 687 (2010).

[6] J. J. Pla, K. Y. Tan, J. P. Dehollain, W. H. Lim, J. J. L. Morton, F. A. Zwanenburg, D. N. Jamieson, A. S. Dzurak, and A. Morello, *Nature* **496**, 334 (2013).

[7] H. Morishita, L. S. Vlasenko, H. Tanaka, K. Semba, K. Sawano, Y. Shiraki, M. Eto, and K. M. Itoh, *Phys. Rev. B* **80**, 205206 (2009).

[8] D. P. Franke, F. Hoehne, L. S. Vlasenko, K. M. Itoh, and M. S. Brandt, *Phys. Rev. B* **89**, 195207 (2014).

[9] L. Dreher, F. Hoehne, H. Morishita, H. Huebl, M. Stutzmann, K. M. Itoh, and M. S. Brandt, *Phys. Rev. B* **91**, 075314 (2015).

[10] A. M. Tyryshkin, S. A. Lyon, A. V. Astashkin, and A. M. Raitsimring, *Phys. Rev. B* **68**, 193207 (2003).

[11] A. M. Tyryshkin, S. Tojo, J. J. L. Morton, H. Riemann, N. V. Abrosimov, P. Becker, H.-J. Pohl, T. Schenkel, M. L. W. Thewalt, K. M. Itoh, and S. A. Lyon, *Nature Mater.* **11**, 143 (2012).

[12] K. Saeedi, S. Simmons, J. Z. Salvail, P. Dluhy, H. Riemann, N. V. Abrosimov, P. Becker, H.-J. Pohl, J. J. L. Morton, and M. L. W. Thewalt, *Science* **342**, 830 (2013).

[13] K. M. Itoh and H. Watanabe, *MRS Commun.* **4**, 143 (2014).

[14] F. R. Bradbury, A. M. Tyryshkin, G. Sabouret, J. Bokor, T. Schenkel, and S. A. Lyon, *Phys. Rev. Lett.* **97**, 176404 (2006).

[15] C. C. Lo, S. Simmons, R. L. Nardo, C. D. Weis, A. M. Tyryshkin, J. Meijer, D. Rogalla, S. A. Lyon, J. Bokor, T. Schenkel, and J. J. L. Morton, *Appl. Phys. Lett.* **104**, 193502 (2014).

[16] G. Wolfowicz, M. Urdampilleta, M. L. W. Thewalt, H. Riemann, N. V. Abrosimov, P. Becker, H.-J. Pohl, and J. J. L. Morton, *Phys. Rev. Lett.* **113**, 157601 (2014).

[17] A. Laucht, J. T. Muhonen, F. A. Mohiyaddin, R. Kalra, J. P. Dehollain, S. Freer, F. E. Hudson, M. Veldhorst, R. Rahman, G. Klimeck, K. M. Itoh, D. N. Jamieson, J. C. McCallum, A. S. Dzurak, and A. Morello, *Sci. Adv.* **1**, e1500022 (2015).

[18] F. Hoehne, L. Dreher, M. Suckert, D. P. Franke, M. Stutzmann, and M. S. Brandt, *Phys. Rev. B* **88**, 155301 (2013).

[19] L. Dreher, F. Hoehne, M. Stutzmann, and M. S. Brandt, *Phys. Rev. Lett.* **108**, 027602 (2012).

[20] F. Hoehne, L. Dreher, D. P. Franke, M. Stutzmann, L. S. Vlasenko, K. M. Itoh, and M. S. Brandt, *Phys. Rev. Lett.* **114**, 117602 (2015).

[21] D. Karaiskaj, M. L. W. Thewalt, T. Ruf, M. Cardona, H.-J. Pohl, G. G. Deviatyach, P. G. Sennikov, and H. Riemann, *Phys. Rev. Lett.* **86**, 6010 (2001).

[22] A. Yang, M. Steger, D. Karaiskaj, M. L. W. Thewalt, M. Cardona, K. M. Itoh, H. Riemann, N. V. Abrosimov, M. F. Churbanov, A. V. Gusev, A. D. Bulanov, A. K. Kaliteevskii, O. N. Godisov, P. Becker, H.-J. Pohl, J. W. Ager, and E. E. Haller, *Phys. Rev. Lett.* **97**, 227401 (2006).

[23] A. Yang, M. Steger, T. Sekiguchi, M. L. W. Thewalt, T. D. Ladd, K. M. Itoh, H. Riemann, N. V. Abrosimov, P. Becker, and H.-J. Pohl, *Phys. Rev. Lett.* **102**, 257401 (2009).

[24] M. Steger, T. Sekiguchi, A. Yang, K. Saeedi, M. E. Hayden, M. L. W. Thewalt, K. M. Itoh, H. Riemann, N. V. Abrosimov, P. Becker, and H.-J. Pohl, *J. Appl. Phys.* **109**, 102411 (2011).

[25] J. Z. Salvail, P. Dluhy, K. J. Morse, M. Szech, K. Saeedi, J. Huber, H. Riemann, N. V. Abrosimov, P. Becker, H.-J. Pohl, and M. L. W. Thewalt, *Phys. Rev. B* **92**, 195203 (2015).

[26] C. C. Lo, M. Urdampilleta, P. Ross, M. F. Gonzalez-Zalba, J. Mansir, S. A. Lyon, M. L. W. Thewalt, and J. J. L. Morton, *Nature Mater.* **14**, 490 (2015).

[27] G. Feher, *Phys. Rev.* **114**, 1219 (1959).

[28] W. G. Breiland, C. B. Harris, and A. Pines, *Phys. Rev. Lett.* **30**, 158 (1973).

[29] H. Huebl, F. Hoehne, B. Grolik, A. R. Stegner, M. Stutzmann, and M. S. Brandt, *Phys. Rev. Lett.* **100**, 177602 (2008).

[30] H. Y. Carr and E. M. Purcell, *Phys. Rev.* **94**, 630 (1954).

[31] J. Medford, L. Cywiński, C. Barthel, C. M. Marcus, M. P. Hanson, and A. C. Gossard, *Phys. Rev. Lett.* **108**, 086802 (2012).

[32] A. S. Kaminskii, V. Karasyuk, and Y. E. Pokrovskii, *Sov. Phys. JETP*, **52**, 211 (1980).

[33] P. Dluhy, J. Z. Salvail, K. Saeedi, M. L. W. Thewalt, and S. Simmons, *Phys. Rev. B* **91**, 195206 (2015).